Continuous chiral resolution of racemic Ibuprofen by diastereomeric salt formation in a Couette-Taylor crystallizer

Laureline Marc, Sabrina Guillemer, Jean-Marie Schneider, Gérard Coquerel

Continuous chiral resolution of racemic Ibuprofen by diastereomeric salt formation in a Couette-Taylor crystallizer

Laureline Marc[1,2], Sabrina Guillemer[2], Jean-Marie Schneider[2], Gérard Coquerel[1,*]

[1] SMS EA3233 Université de Rouen Normandie, Place Emile Blondel, 76821 Mont-Saint-Aignan, France

[2]Seqens Porcheville, 2-8 rue de Rouen, 78440 Porcheville, France

***Corresponding author:** gerard.coquerel@univ-rouen.fr

Abstract

S-Ibuprofen has been proved to be more efficient than racemic Ibuprofen, one the best sell drugs over the world. Thus, there is a strong interest in implementing chiral resolution of racemic Ibuprofen in the continuous mode.

Chiral resolution by diastereomeric salt formation of racemic Ibuprofen has been successfully implemented in a Couette-Taylor (CT) crystallizer. Among the seven parameters identified as impacting, a screening has been performed on the four factors expected to have the strongest influence: temperature gradient in the CT crystallizer, rotation speed, residence time and target temperature within the crystallizer.

Thanks to the rationalization of the study through a design of experiments approach, only 14 distinct experiments were performed to identify the influence of these factors on global productivity/yield, diastereomeric excess and diastereomeric productivity/yield, and to find a first operating point.

If the obtained yields were unsurprisingly low, global productivity and diastereomeric productivity are increased by 16 and 8 times respectively, in comparison with batch mode. Also, continuous mode gives an easy access to a higher diastereomeric excess, in a repeatable manner.

Surprisingly, under the selected process conditions, the steady state does not seem to be reached before 14-15 residence times, which is longer than expected from previous results.

Keywords

Continuous chiral resolution; Couette-Taylor; Ibuprofen; chiral resolution by diastereomeric salt formation; design of experiments

1 Introduction

1.1 Comparison between continuous and batch modes

Continuous chemical processes have been used for decades in the petrochemical and bulk chemical industry, but its development in the pharmaceutical industry is more recent (Badman et al., 2019; Hughes, 2020). In fact, traditionally, active pharmaceutical ingredient (API) production is performed through batch processes. However, batch facilities age and are eventually decommissioned, which can give the opportunity for companies to invest in continuous systems (Cole and Johnson, 2018).

This conversion may be really interesting on an economic aspect, as batch mode has high requirements in terms of human intervention and operating costs (Zhang et al., 2017). Conversely, despite its initial expensive implementation, the continuous mode offers lower operating cost and space requirement. Moreover, it can shorten the development period to pilot and/or to commercial production (Hughes, 2018).

Furthermore, batch production mode has shown some weaknesses over the years, especially batch-to-batch product quality variation. Continuous mode ensures constant product quality, or at least less variation (Ma et al., 2020). This latest can be secured thanks to steady state functioning of continuous process device, which enables a better process control (Cole and Johnson, 2018). Also, given the ability of continuous mode to achieve more efficient heat and mass transfers, temperature and mixing are more effective (Hughes, 2020). Thus, optimization and control of residence times lead to less side-product and an enhanced productivity.

These global increases in efficiency lead to improved process results, such as a better and more constant product quality/purity, an improved selectivity and an increased yield (Cole and Johnson, 2018; Baumann et al., 2020; Hughes, 2020). In addition, thanks to an enhanced robustness, continuous processes have been shown to be easier to scale-up and more predictable than batch ones, allowing agile manufacturing (Wood et al., 2019).

Moreover, continuous mode may be a great solution to perform chemistry that is difficult or impossible to implement in batch mode; it also gives an access to ‘greener’ chemistry and safer processes (Rogers and Jensen, 2019; Baumann et al., 2020; Hughes, 2020).

1.2 Continuous crystallization

Among continuous operations, the bottleneck is mainly linked to the isolation steps: crystallization and filtration (Liu et al., 2019). Crystallization is a critical stage in API production as it governs its purity and physical properties.

Continuous crystallization has recently attracted increasing attention because of the enhanced product and process features mentioned in section 1.1 (Wang et al., 2017; Zhang et al., 2017; Wood et al., 2019; Ma et al., 2020).

Nonetheless, due to their sensitivity to temperature, mixing and residence time, the development of crystallization processes in a continuous mode is really challenging. As in many operations of flow chemistry, some technical difficulties can be encountered because of a high risk of incrustation, fouling and blockage (Rivera et al., 2019). One solution to avoid these issues can be the preventive implementation of periodic temperature cycling (Zhang et al., 2017).

In the specific case of continuous crystallization processes, the improvement of the yield can be lacking, but it can be counterbalanced by an increased productivity (Wood et al., 2019; Ma et al., 2020).

In a general view, Zhang et al., 2017 assess two main difficulties regarding the development of crystallization operations in continuous mode: the ability to determine the suitable continuous crystallization process and the ability to choose the appropriate design for the production of the desired crystals. Moreover, there is still a lack of understanding of fundamentals of crystallization (nucleation, growth, polymorphism, crystal structure property relationships), which is why flow chemistry has been more studied than continuous crystallization (Rogers and Jensen, 2019).

There are two main kinds of continuous crystallizers: mixed-suspension, mixed-product removal (MSMPR) crystallizers and plug flow crystallizers (PFCs). MSMPR crystallizers are the most used in API development, probably because of their easy handling, but their main issues are the difficulty to control crystal shape and crystal size distribution, and a complicated scale-up. Conversely, PFCs can be easily scaled up and offer a higher efficiency than MSMPR reactors for the same volume; however, they present a higher risk of fouling or blockage, and the equipment is more complex (Zhang et al., 2017; Wood et al., 2019). Wood et al. have interestingly pointed out that no study has been done on a direct comparison between PFCs and MSMPR crystallizers. Theoretically, yield should be higher in PFC-based systems.

Other types of continuous crystallizers have been developed in the past decade, such as continuous oscillatory baffled crystallizers, fluidized bed crystallizers or continuous laminar shear crystallizers (Wang et al., 2017; Wood et al., 2019).

Continuous laminar shear crystallizers are constituted of two temperature-regulated concentric cylinders. The flow goes through the gap between the two cylinders, and the rotation of the external cylinder creates a shear force. Couette-Taylor (CT) crystallizers have the same constituents than laminar shear crystallizers, except that the rotating cylinder is the internal one, the outer cylinder being at rest.

1.3 Continuous Couette-Taylor crystallizer

The fluid flow between two concentric cylinders has been studied and described by Couette in 1890 (Couette, 1890). Hydrodynamic instability occurrence in the flow was observed by various scientists when the rotation speed was sufficient. One century ago, Taylor explained the nature of this instability by highlighting the existence of specific vortices in the liquid (Taylor, 1923). These vortices are caused by the sudden predominancy of the centrifugal forces over viscous forces (Kim, 2014). This specific flow motion has been studied theoretically and/or experimentally by many groups afterwards (Chandrasekhar, 1961; Sparrow et al., 1964; Donnelly and Schwarz, 1965; Kataoka, 1986; Maron and Cohen, 1991). The two latter authors detected the potential use as chemical reactor of device with such characteristic fluid flow, as it can be considered as a series of micro-stirred tanks.

Continuous CT crystallizers have been developed based on these flow characteristics: at low rotation speed, the fluid follows a laminar Couette motion. When increasing the rotation speed beyond a certain critical value, the flow changes into radial vortex combined with small axial dispersion: this is the Couette-Taylor vortex (Kim, 2014). Figure 1 displays the flow induced by the rotation of the internal cylinder in a CT crystallizer: a stratified Couette flow coupled with Taylor vortices.

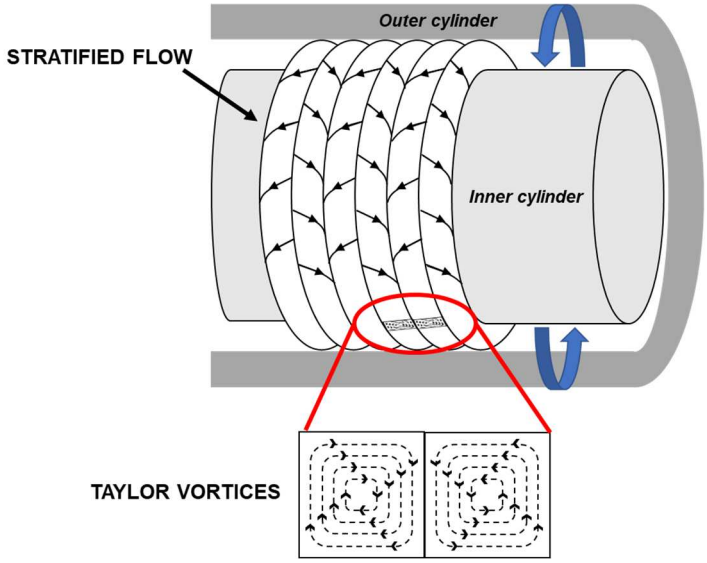

Figure 1: Visualization of the Taylor vortices in a CT crystallizer

The critical rotation speed can be retrieved from the critical Taylor number Ta (Taylor, 1923), which can be described as the ratio of centrifugal forces to viscous forces (Kim, 2014). Ta is given by Equation (1):

$$Ta = \frac{\Omega_i^2 r_i d^3}{\nu^2} \qquad (1)$$

In Equation (1), Ω_i is the rotation speed of the inner cylinder (rad/s), d the gap space between the two cylinders (m) and ν the kinematic viscosity (m²/s).

At some specific critical Taylor number 'multiples', the initial axisymmetric Taylor vortex flow goes through other flow regimes up to a full turbulent flow: (a) laminar Couette flow, (b) laminar periodic Taylor vortex flow, (c) singly periodic wavy vortex flow, (d) doubly periodic wavy vortex flow, (e) weakly turbulent wavy vortex flow, (f) turbulent vortex flow, (g) turbulent aperiodic flow (Kataoka, 1986; Maron and Cohen, 1991). Each flow regime has a unique influence on the crystallization course (Kim, 2014). The advantage of CT crystallizer is that the switch from one flow regime to another is easily reachable by changing the rotation speed (Wang et al., 2017).

The azimuthal fluid motion resulting from the rotation of the inner cylinder of CT crystallizers creates periodic toroidal vortex flow patterns; such patterns give the CT crystallizers an ability for a highly efficient and homogeneous mixing (Kang et al., 2003).
Owing to this improved mixing effect in the Taylor vortices, the fluid motion shows enhanced heat and mass transfer rates, in comparison with the turbulent flow of batch tanks or even of other continuous crystallizers (Maron and Cohen, 1991; Kang et al., 2003; Kim, 2014; Wu et al., 2015; Nguyen et al., 2017). Since the crystal properties are dependent on the operating conditions, thus on the hydrodynamic crystallization conditions, the CT crystallizer seems to be a suitable device for the implementation of various continuous crystallization processes (Nguyen et al., 2010; Wang et al., 2017).
Moreover, the design of such device can be adapted, for example by using a multiple-feeding mode (Nguyen et al., 2012), or by implementing a temperature regulation of each cylinder (Wu et al., 2015). Besides its efficiency in controlling crystal size distribution (CSD), Wu et al. (2017) assessed the use of CT crystallizers in the non-isothermal mode as "especially appropriate for cooling crystallization".

General quality requirements for pharmaceutical crystallization are yield, purity, size, morphology, polymorphism, and chirality (Zhang et al., 2017; Liu et al., 2019). Special fluid motion of CT crystallizers has proved its impact in crystallization processes on particle size distribution (PSD) (Wu et al., 2015; Nguyen et al., 2017; Wu et al., 2017), morphology, agglomeration (Thai et al., 2015) and polymorphism (Nguyen et al., 2010; Nguyen et al., 2012; Park et al., 2015). More recently, the use of CT crystallizers in non-isothermal mode has shown its ability to hasten deracemization processes (Kim et al., 2017; Schindler, 2020). In parallel, the same technology was also used for *mechanical* continuous chiral resolution (Hermans et al., 2017; Marichez et al., 2019).

1.4 Continuous chiral resolution

Enantiomers are stereoisomer molecules that are mirror images of each other, thus non superimposable (e.g., a pair of hands). The chirality of such molecules has a great importance in the pharmaceutical industry since only one enantiomer (eutomer) of a chiral

drug provides the best therapeutic effect and/or less side effects. The other enantiomer (distomer) is generally less/not efficient, or even harmful (Lorenz et al., 2020).

There are different ways to access pure chiral molecules, such as stereoselective synthesis, chromatography, biocatalytic synthesis or crystallization. Chromatography techniques are very convenient but also quite expensive, hence, except for few applications, inapplicable for large scale processes. Conversely, resolution by crystallization ranks as the oldest and most readily applicable operation in chemical processing (Siedlecka, 2013). There are many techniques of chiral resolution by crystallization; among them, one of the easiest to implement and to scale up is the chiral resolution by diastereomeric salt formation, also called Pasteurian resolution (Wang and Chen, 2013).

Diastereomeric salt formation, is the most classical resolution technique involving crystallization. This method breaks the symmetry among the enantiomers (Fogassy et al., 2006; Faigl et al., 2008; Wang and Chen, 2013). By reacting a single enantiomer of a chiral resolving agent (RA) on the couple of enantiomers to resolve, a dissymmetric par of diastereomeric salts is formed. This reaction is based on an opposite acid-base character between the enantiomers and the RA. After salt formation, the diastereomers can be separated: unlike enantiomers, diastereomers have different physical properties, such as solubility. Therefore, it is easier to separate diastereomers than enantiomers (Coquerel, 2015; Viedma et al., 2015).

Ibuprofen is a chiral drug currently marketed in its racemic form, i.e., a 1:1 mixture of S-(+)-Ibuprofen (S-Ibu) and R-(-)-Ibuprofen (R-Ibu) (Figure 2). However, there are clear clinical benefits of using S-Ibu instead of racemic Ibuprofen (rac-Ibu) as it appeared to be more efficient (Evans, 2001).

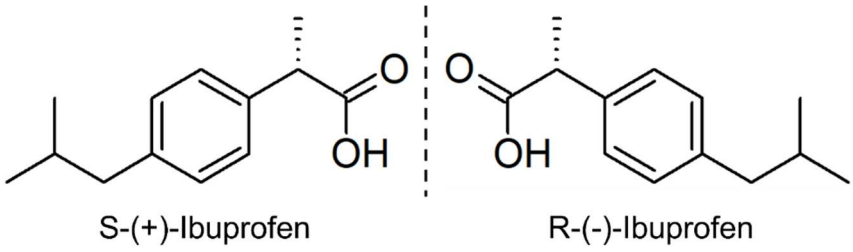

Figure 2: Enantiomers of Ibuprofen

Classically, racemic Ibuprofen can be resolved through a diastereomeric salt formation with S-(+)-Lysine followed by another step of separation, such as recrystallization or temperature selective diastereo-recognition (Bhattacharya and Murphy, 2003; Carvalho et al., 2006). The S-(+)-Lysine should then be removed by a salting out in order to recover S-Ibu enantiomer.

The test of S-(-)-α-Methylbenzylamine (S-αMBA) as a resolving agent can be interesting, as it offers the possibility to perform an efficient chiral recognition in the solid state for numerous acidic enantiomers. However, by contrast to L-lysine the S-αMBA should be carefully

removed afterwards, as it is not a GRAS (Generally Regarded As Safe) substance, i.e. unsuitable as a component for drug formulations. It can be easily eliminated by adding an acid to the diastereomeric salt dissolved in ethanol. Despite this inconvenience, S-αMBA remains a remarkable resolving agent of carboxylic acids (Lemmerer et al., 2010).

In the present work, the resolution of rac-Ibu is performed with S-αMBA in a mixture ethanol/water 80/20 w/w (Scheme 1). Previous work has been performed in pure ethanol, but chiral purity was low, and the filtration was difficult because of the needle shaped crystals. Batch study showed that the addition of water enhanced the diastereomeric purity and has changed the crystal morphology from needles to platelets (Marc et al., 2021), which are more suitable for filtration and conveyance.

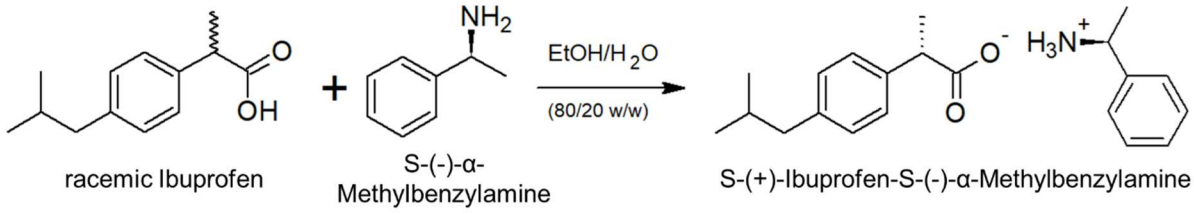

Scheme 1: Chiral resolution of racemic Ibuprofen by diastereomeric salt formation with S-α-Methylbenzylamine, the R-Ibu-S-αMBA should remain in solution

Rac-Ibu being one of the best-selling pharmaceutical molecules in the world, there is great interest in developing its continuous chiral resolution to produce the more efficient single enantiomer S-Ibu.

Chiral resolution by continuous crystallization processes are rarely reported in the literature, but examples of preferential crystallization (PC) implemented in MSMPR crystallizers and in fluidized bed crystallizers have been found (Wang et al., 2017; Lorenz et al., 2020; Ma et al., 2020). This lack of published studies may come from the general low yield recovered in continuous chiral resolution by crystallization processes (Zhang et al., 2017).

The specific fluid motion features of CT crystallizers and the results obtained for deracemization processes are promising regarding the implementation of chiral resolution by crystallization processes in CT crystallizers.

Continuous or semi-continuous mode have already been successfully applied to chiral resolution of rac-Ibu with enzyme resolution techniques in a packed bed reactor operating as a plug-flow reactor (Sánchez et al., 2000) or in an enzymatic membrane reactor considered as a continuous stirred tank reactor (Long et al., 2005), and with PC of the diastereomer (±)-Ibuprofen-S-Lysine through a sequential coupled-batch operation (Simon et al., 2019).

The present study aims at evaluating the transfer from batch mode to continuous mode in a CT crystallizer of racemic Ibuprofen resolution by diastereomeric salt formation with S-αMBA, in a mixture ethanol/water 80/20 w/w. Regarding the number of parameters

potentially impacting the process results (yield, product quality,…), this work has been rationalized through a Design of Experiments (DoE) presented in section 3.

2 Material and methods

2.1 Continuous set-up

The set-up to perform the continuous chiral resolution in the CT crystallizer is depicted in Figure 3. The 100 mL CT crystallizer, manufactured by Laminar Co., Ltd, is placed horizontally to eliminate any hydrostatic pressure effect (Kang et al., 2003). The inner cylinder ($r_i = 19.5$ mm) can rotate while the outer ($r_o = 23.4$ mm) is at rest. The gap width between the two cylinders d is 3.9 mm.

The two cylinders are temperature-regulated independently, with $T1$ the set temperature of the thermostat of the inner cylinder and $T2$ the set temperature of the thermostat of the outer cylinder. Thus, the reactor can be used in the non-isothermal mode (Wu et al., 2015). The temperature of the inner and outer cylinders is respectively controlled using a Lauda Proline RP890 and a Lauda Proline RP845, filled with ethylene glycol/water 40/60 V/V.

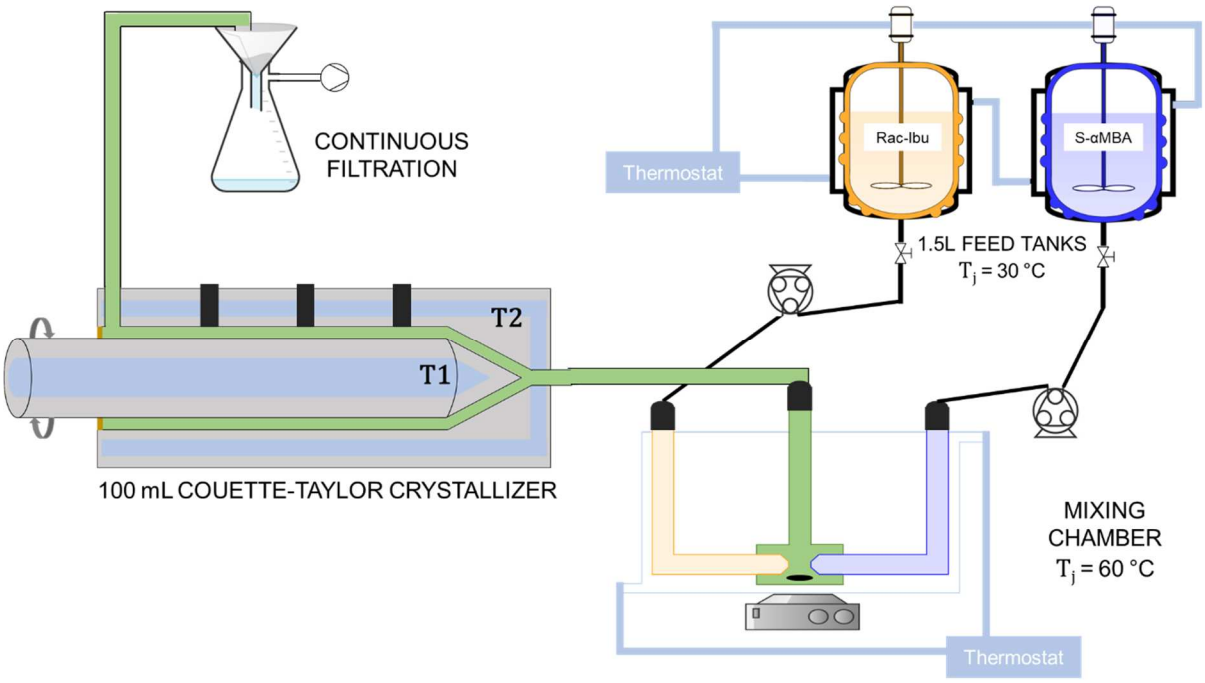

Figure 3: Couette-Taylor crystallizer continuous set-up

The design of the feeding part (right side of Figure 3) was complex because it needed to comply with various constraints: (i) after a preliminary experiment, it has been found that the CT crystallizer should be fed with a solution rather than a suspension. (ii) as experiments can take several hours, there is a risk of precipitation if the rac-Ibu and the S-αMBA are stored in the same feed tank at a temperature below 40°C. (iii) in order to avoid any chemical

degradation, the starting material should not be maintained at hot temperature for hours. The solution to this threefold problem, was then to separate rac-Ibu and S-αMBA in two different feed tanks with a temperature regulation at 30 °C, ensured by a Lauda Eco RE420.
In order to gather, mix and heat the two feeding solutions before entering the CT crystallizer, a doubled-jacketed special mixing chamber has been designed. For all experiments, this chamber was regulated at 60 °C and it ensured an efficient mixing by using a magnetic stirrer.

The solutions of rac-Ibu and S-αMBA were transported from the feed tanks to the CT crystallizer, by passing through the mixing chamber, by using a peristaltic pump Ismatec ISM833C. Chiral resolution by crystallization then occurred in the CT crystallizer, and the product was collected and filtered *in situ* on a sintered glass filter. The recovered product was dried at 50 °C for 12 h before performing the analyses described in the following sections.

Residence times, temperatures and rotation speeds were defined according to the desired values of the DoE (see section 3).

2.2 X-Ray Power Diffraction (XRPD)

XRPD measurements were carried out on a Bruker D8 Discover apparatus, using the Cu Kα radiation (1.54 Å). The samples were scanned from 3 to 30° 2θ angles, with a 0.04° step (0.5 s duration). The detector slit was set at 0.6 mm. The software used to process the data is Bruker DIFFRAC.EVA V4.1.

2.3 Chiral High Performance Liquid Chromatography (HPLC)

The chiral HPLC analyses were performed on a Thermoscientific system with Ultimate 3000 modules (Pump, Autosampler, RS variable wavelength detector) with a chiral column Daicel Chiralcel OD-H 5 µm 250-4.6 mm and the following conditions:

- Mobile phase: n-heptane/propan-2-ol/trifluoroacetic acid 100/1/0.1
- Flow rate: 1 mL/min
- Wavelength: 225 nm
- Volume injected: 5 µL
- Oven temperature: 25 °C

Samples were dissolved in the mobile phase. The software used to process the data is Thermo Scientific Dionex Chromeleon 6.8 Chromatography Data System.

2.4 Materials

Rac-Ibu has been supplied by Pharmadev, S-αMBA and HPLC trifluoroacetic acid by Acros Organics, HPLC n-heptane by Fisher and technical ethanol, technical ethylene glycol and HPLC propan-2-ol by VWR.

3 Construction of the Design of Experiments (DoE)

In the presented work, many process conditions can have an impact on the product features (yield, chiral purity…). Regarding that, the use of a DoE seems necessary to rationalize the study, in order to obtain a robust operating point. The effectiveness of such tool has already been proved when dealing with process study with several impacting parameters (Sánchez et al., 2000).

In the current study, seven parameters have been identified as potentially impacting factors. They deal with the features offered by the CT crystallizer (parameters (1), (2), (3) and (5)), with the continuous mode (parameter (4)) and with the crystallization process (parameters (6) and (7)):

- (1) Absolute temperature difference between the two cylinders |ΔT|, with $|\Delta T| = |T1 - T2|$
- (2) Sign of ΔT, i.e., which cylinder is the cold part when the other is the hot one,
- (3) Rotation speed Ω,
- (4) Residence time t, i.e., flowrate,
- (5) Reference temperature T_{ref}, i.e., target temperature within the CT crystallizer, with $T_{ref} = \frac{T1+T2}{2}$.
- (6) Medium concentration,
- (7) Solvent mass ratio EtOH/H_2O.

In order to make a primary outline of the influence of the different parameters, and to identify the optimization levers for further development, a first screening has been set up with the parameters related to the CT crystallizer and to the continuous mode, assessed to be the most impacting ones. Parameters (1) and (2) have been gathered as one factor, which results in a screening of four factors:

- (1)(2) Temperature difference ΔT, with $\Delta T = T1 - T2$
- (3) Rotation speed Ω,
- (4) Residence time t, i.e., flowrate,
- (5) Reference temperature T_{ref}, i.e., target temperature within the CT crystallizer, with $T_{ref} = \frac{T1+T2}{2}$.

For this first experimental design, the medium concentration was fixed at 57 mg/mL, and the mass ratio EtOH/H_2O at 80/20. The medium was not highly concentrated in order to avoid any fouling in this first set of experiments.
For each factor, three levels were determined. The following sections detail the choice of the factor levels, which was a critical step in the DoE construction. They had to be sufficiently distinct and not too close to each other to obtain significantly different and informative results.

3.1 Choice of the factor levels

3.1.1 Temperature difference ΔT (°C)

This factor is a mix of the factors (1) - absolute temperature difference |ΔT| - and (2) - sign of ΔT -. Its definition can be found in Equation (2) with T1 the set temperature of the thermostat of the inner cylinder and T2 the set temperature of the thermostat of the outer cylinder.

$$\Delta T = T1 - T2 \quad (2)$$

The chosen levels were: -10 °C; 0 °C; +10 °C. Sign '-' refers to the inner cylinder being the cold part and the outer cylinder being the hot one; sign '+' refers to the reverse situation. The sign of ΔT can have a strong impact on the product features, as shown by Wu et al. (2015).
The investigation of this 3-level factor will reveal the potential advantage of applying a temperature gradient within the CT crystallizer for the studied system, and if there is, what is its best orientation.

3.1.2 Rotation speed Ω (rpm)

To ensure the unique flow motion of the CT crystallizer with Taylor vortices, the rotation speed Ω should be above the critical Taylor number. This latest then needs to be calculated in a first place.

Calculation of the critical Taylor number

The critical Taylor number depends on the kinematic viscosity of the system and on the geometry of the CT crystallizer, characterized by the ratio d/r_i , or by the radius ratio $\eta = r_i/r_o$.
In the used CT crystallizer, $\eta = 0.83$, which gives a critical Taylor number of 1902, according to Donnelly and Schwarz (1965). However, this critical Taylor number does not consider the presence of an axial flow. In this case, a correction should be made (Maron and Cohen, 1991):

$$Ta^*_c = Ta^*_c(Re_z = 0) + 26.5{Re_z}^2 \quad (3)$$

In Equation (3), Ta^*_c is the critical Taylor number with the axial flow and Ta^*_c $(Re_z = 0)$ the critical Taylor number without the axial flow. Re_z is defined in Equation (3)

$$Re_z = \frac{dV_m}{\upsilon} \quad (4)$$

In Equation (4), d is the gap width (m), V_m the mean axial linear velocity (m/s) and ν the kinematic viscosity (m²/s). Kinematic viscosity of the medium was measured at 30 °C: 2.55 mm²/s. This gives $Ta^*_c = 1927$, 1905 and 1903 for respective residence times of 5 min, 15 min and 30 min (see section 3.1.3). The proposed correction appears to be negligeable, even for short residence times.

Table 1 gives the rotation speed range for each CT flow regime (Kataoka, 1986). According to the residence time (5, 15 or 30 min) the boundary rotation speeds differ from 1 to 5 units; the values displayed in Table 1 are those for a residence time of 15 min. Three flow regimes were chosen to be studied with rotation speeds of: 200 rpm, 500 rpm and 1000 rpm.

Ta/Ta^*_c	**Flow regime**	**Rotation speed range (rpm)**
$Ta/Ta^*_c < 1$	Laminar Couette flow	$\Omega < 31$
$1 < Ta/Ta^*_c < 9$	Laminar periodic Taylor vortex flow	$31 < \Omega < 94$
$9 < Ta/Ta^*_c < 176.89$	Singly periodic wavy vortex flow **↳To study with 200 rpm**	$94 < \Omega < 416$
$176.89 < Ta/Ta^*_c < 324$	Doubly periodic wavy vortex flow **↳To study with 500 rpm**	$416 < \Omega < 563$
$324 < Ta/Ta^*_c < 1089$	Weakly turbulent wavy vortex flow **↳To study with 1000 rpm**	$563 < \Omega < 1032$
$1089 < Ta/Ta^*_c < 25600$	Turbulent vortex flow	$1032 < \Omega < 5003$
$25600 < Ta/Ta^*_c$	Turbulent aperiodic flow	$5003 < \Omega$

Table 1: Taylor number and rotation speed ranges of each flow regime encountered in the used CT crystallizer for a residence time of 15 min. Among the mentioned flow regimes, three will be studied: the singly periodic wavy vortex flow (Ω = 200 rpm), the doubly periodic wavy vortex flow (Ω = 500 rpm) and the weakly turbulent wavy vortex flow (Ω = 1000 rpm).

3.1.3 Residence time t (min)

In the literature, residence time in CT crystallizer typically ranges between 1 min to 60 min (Nguyen et al., 2010). Regarding feasibility aspects, it has been chosen to study: 5 min, 15 min and 30 min.

3.1.4 Reference temperature T_{ref}, or target temperature within the CT crystallizer (°C)

In the continuous set-up presented in Figure 3, temperatures within the CT reactor are monitored directly by the thermostats of the two cylinders. Nevertheless, the average temperature inside the CT crystallizer impacts the results, but this temperature cannot be monitored directly. However, in the DoE experimental approach, the chosen factors must be precisely controlled and independent one to each other. Therefore, in order to study different temperatures of crystallization, a reference temperature T_{ref}, related to the thermostat set temperatures, must be introduced. It is defined in Equation (5), with $T1$ the set temperature of the inner cylinder thermostat and $T2$ the set temperature of the outer cylinder thermostat.

$$T_{ref} = \frac{T1 + T2}{2} \tag{5}$$

Thereby, for each experiment, the inner cylinder thermostat set temperature and that of the outer cylinder thermostat are imposed by the values of T_{ref} and ΔT chosen for the experiment, T_{ref} and ΔT factors remaining independent one to each other.

Previous batch study was performed with a cooling crystallization to 20 °C. In the continuous DoE, it has been decided to experiment the same value as in batch mode: 20 °C, one value above and one value below. Thus, the effect of the increase and of the decrease of the final temperature could be studied. In the end, the chosen values of T_{ref} were: 15 °C, 20 °C and 25 °C.

The investigated factors and levels are summed up in Table 2.

X	Name of the factor	Level	Value of the level
X1	Temperature difference ΔT	0	-10 °C
		1	0 °C
		2	+10 °C
X2	Rotation speed Ω	0	200 rpm
		1	500 rpm
		2	1000 rpm
X3	Residence time t	0	5 min
		1	15 min
		2	30 min
X4	Temperature inside the CT crystallizer T_{ref}	0	15 °C
		1	20 °C
		2	25 °C

Table 2: Factors and levels of the DoE

3.2 Matrix of experiments

After the determination of each factor level, the DoE matrix of experiments was built with the 'Screening' tool of Azurad® software (AZURAD SAS, France; Basic version 1.3.4). By using an exchange algorithm, a D-optimal matrix of 10 experiments was chosen with minimal inflation factors on the model coefficient (experiments 1 to 10 in Table 3).

The analysis of these first experiments led to the implementation of 4 more experiments (including 2 repetitions). The full matrix of experiments and its corresponding experimentation plan can be found in Table 3.

Experiment	Repetition	Matrix of experiments				Experimentation plan			
		X1	*X2*	*X3*	*X4*	*ΔT (°C)*	*Ω (rpm)*	*t (min)*	*T_{ref} (°C)*
1	2	2	0	0	0	10	200	5	15
2	1	0	2	2	0	-10	1000	30	15
3	1	0	1	0	1	-10	500	5	20
4	1	1	1	1	0	0	500	15	15
5	2	2	2	1	1	10	1000	15	20
6	1	1	0	2	1	0	200	30	20

7	1	0	0	1	2	-10	200	15	25
8	1	1	2	0	2	0	1000	5	25
9	1	2	1	2	2	10	500	30	25
10	1	2	2	2	2	10	1000	30	25
11	2	0	2	1	2	-10	1000	15	25
12	2	1	2	0	0	0	1000	5	15
13	1	0	2	0	0	-10	1000	5	15
14	1	2	2	0	0	10	1000	5	15

Table 3: DoE matrix of experiments and its corresponding experimentation plan, constructed with the 'Screening' tool of the software Azurad®. Experiments 1 to 10 are part of the initial DoE construction. Experiments 11 to 14 were performed after the analysis of experiments 1 to 10.

3.3 Samples collection

Previous results in pure ethanol predicted the quick access to the steady state functioning in the CT crystallizer, as shown in Figure 4.

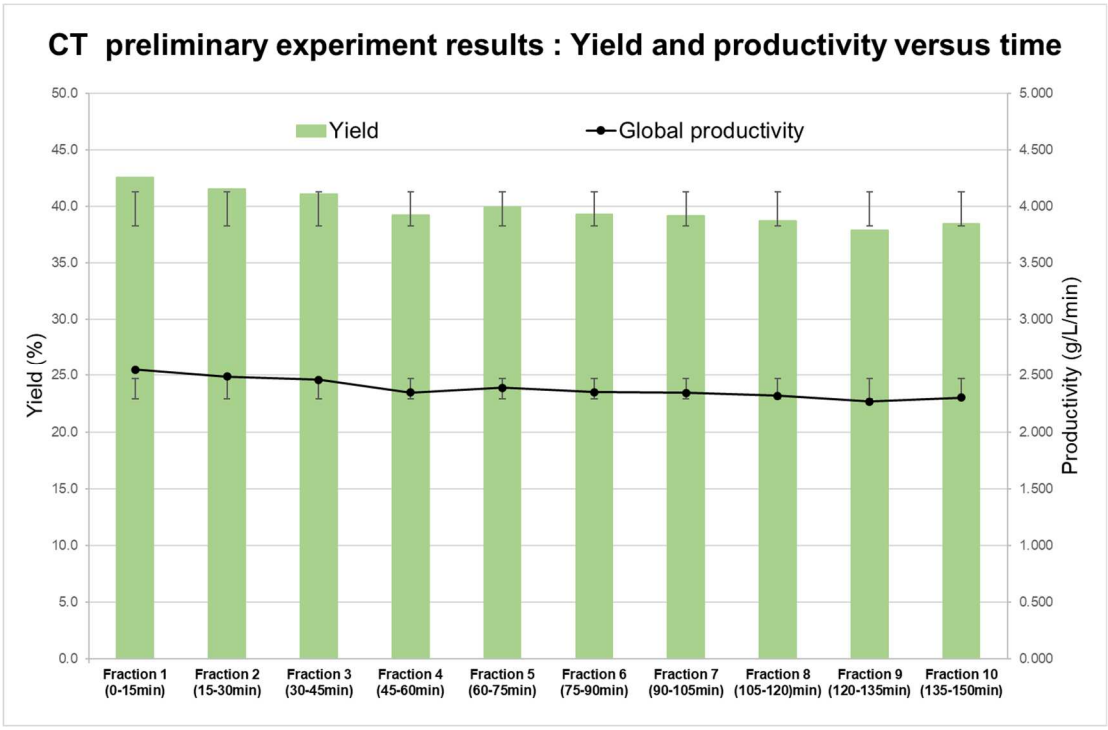

Figure 4: Example of the yield and productivity versus time of a chiral resolution using CT crystallizer in non-isothermal mode. Samples (fractions) were collected every 15 min (= residence time). Green (histogram): yield (%); Black (line): productivity (g/L/min)

Regarding that, experiments lasted 10 residence times. Every fraction (product recovered in 1 residence time) was collected, but only fractions 3 (2 to 3 residence times), 5 (4 to 5 residence times) and 8 (7 to 8 residence times) were analyzed.

3.4 Responses

In this screening, five responses have been considered to study the influence of the different factors on the product features:

- Global productivity (g/L/min)
- Global yield (%)
- Diastereomeric excess
- Diastereomeric productivity (g/L/min)
- Diastereomeric yield (%)

As the present work deals with continuous chiral resolution, productivity, yield and diastereomeric excess are crucial results. They represent the efficiency of the process in the continuous mode.

Productivity is defined in Equation (6), with $m_{collected}$ the mass of the solid recovered from V, the volume of suspension collected during $t_{collection}$, the duration of the fraction collection.

$$Productivity = \frac{m_{collected}}{V * t_{collection}} \quad (6)$$

Yield is defined in Equation (7), with $m_{expected}$ the maximum mass of solid that can be recovered from V during $t_{collection}$.

$$Yield = \frac{m_{collected}}{m_{expected}} * 100 \quad (7)$$

The diastereomeric excess (de) defines the amount of S-Ibu-S-αMBA recovered 'alone'. It can be calculated as:

$$de = [(S-Ibu-S-\alpha MBA) - (R-Ibu-S-\alpha MBA)] \,/\, [\,(S-Ibu-S-\alpha MBA) + (R-Ibu-S-\alpha MBA)] \quad (8)$$

Diastereomeric excess defines the process effectiveness in separating S-Ibu and R-Ibu.

Global productivity and global yield refer to the whole recovered product, which include S-Ibu-S-αMBA and R-Ibu-S-αMBA. Therefore, the diastereomeric productivity and the diastereomeric yield must be introduced, in order to define the real production in the desired diastereomer.

The analysis of these different responses with the DoE tool can assess a 'weight' of impact for every factor investigated, and a first outline of their best level(s).

4 Results and Discussion

For each experiment of Table 3, the mass of the recovered product was measured for every fraction, but chiral purity was only analyzed for fractions 3, 5 and 8 (see section 3.3). XRPD analysis was also performed on these fractions. All the analyzed samples showed the correct solid phase. As an example, XRPD diffractograms of experiment 2 can be found in

the supplementary materials. They are compared with the rac-Ibu (starting material), the pure S-Ibu-S-αMBA and with the calculated diffractogram (obtained from the data at 173 K of Lemmerer et al., 2010). The products obtained from chiral resolution exhibit small peak shifts compared with the pure material collected at room temperature. They are due to the presence of a partial solid solution enriched in S-Ibu-S-αMBA (Marc et al., 2021).

Surprisingly, the yield profile over the 10 fractions collected (one per residence time) was not as expected (Figure 4). This will be discussed in section 4.3. At the same time, the patterns on repeated trials being very similar, this does not appear to be due to experimental error in implementation of sampling or analysis. Therefore, it was decided to analyze the average of the results of fractions 3, 5 and 8 for each response. They can be found in Table 4.

Experiment	Global productivity (g/L/min)	Global yield (%)	Diastereomeric excess	Diastereomeric productivity (g/L/min)	Diastereomeric yield (%)
1 R1	1.317	14.7	0.53	1.139	6.3
1 R2	1.103	12.1	0.54	0.997	5.5
2	0.085	5.8	0.69	0.093	3.1
3	1.623	15.9	0.62	1.986	10.9
4	0.626	18.8	0.58	0.736	12.2
5 R1	0.135	4.3	0.70	0.151	2.5
5 R2	0.232	7.2	0.68	0.284	4.7
6	0.151	11.1	0.67	0.217	7.1
7	0.246	6.3	0.70	0.414	6.8
8	1.432	13.9	0.67	1.753	9.6
9	0.006	0.4	0.58	0.006	0.2
10	0.017	1.0	0.64	0.015	0.5
11 R1	0.106	3.5	0.71	0.105	1.7
11 R2	0.773	11.8	0.71	0.539	8.9
12 R1	2.217	22.1	0.58	2.311	12.8
12 R2	3.976	19.6	0.57	1.992	11.0
13	2.688	26.4	0.58	2.883	15.9
14	3.185	15.7	0.59	1.657	9.2

Table 4: Average DoE responses for every experiment. For 'global' results, the average has been calculated with all the fractions; for 'diastereomeric' results, the average has been calculated with the fractions analyzed by chiral HPLC, i.e., fractions 3, 5 and 8. In the column 'Experiment', 'R' stands for repetition.

The statistical analyses and interpretation plot from Azurad® were used to evaluate the reliability of each model and to determine the most impacting parameter among ΔT, Ω, t and T_{ref}, and their preferential set-up regarding each response.

For the individual factor effect evaluation:

- Pareto plots and the total effect plot
- p-values of t test on coefficient

For the model reliability

- R^2 of the model
- p-value of F test on regression
- p-value of F test on lack of fit

In some cases, with such screening design, the simplified model chosen may not be significant while some coefficient effects are significant. Sometimes even, the effects of the factors do not appear to be statistically significant, but Pareto analysis shows that one factor is responsible for the majority of the variability observed. This can happen if significant interaction effects exist.

The influence scores given in Figure 5 to Figure 9 are extrapolated from the Pareto plots (coefficients) provided by Azurad®. As explained above, it is noteworthy to mention that the importance of some factors can be hidden or enhanced because of interactions between them.

4.1 Analysis of the responses

4.1.1 Global productivity

The regression model given by Azurad® is significant with a p-value of 1.6 % and a R^2 of 0.808. The lack of fit is not significant with a p-value of 40 %. For global productivity, the experimental results and the screening model fit quite well.

As shown in Figure 5a, the main impacting factor is the residence time t. Rotation speed Ω has a small influence on global productivity and the temperature difference ΔT and the reference temperature T_{ref} have a poor impact.

The impact of each factor level on the increase of the global productivity can be found in Figure 5b. The interpretation should be moderated regarding the influence of each factor discussed before.

The predominance of $t = 5$ min as global productivity enhancer seems clear. The lower the residence time the higher the global productivity. At small residence times, the cooling is

faster, which increases the nucleation rate. The side effect is the recovery of a crystal population with a broad PSD, i.e., a less homogeneous powder.

Regarding the rotation speed, it appears that the global productivity increases with the rpm. This result is consistent with an enhanced mass transfer for high rotation speed (Nguyen et al., 2010; Park et al., 2015; Nguyen et al., 2017).

The use of the isothermal mode ($\Delta T = 0\,°C$) seems to improve global productivity. Wu et al., 2017 have shown that when increasing the temperature gradient, the nucleation occurs at higher supersaturation. This means that crystallization needs a higher driving force to start. When there is no temperature difference, the nucleation starts 'earlier' and can then results in a higher production of crystals. It can explain why the isothermal mode leads to higher global productivities.

The decrease of T_{ref} seems to have a positive effect on global productivity, which can be expected as supersaturation increases when T_{ref} diminishes.

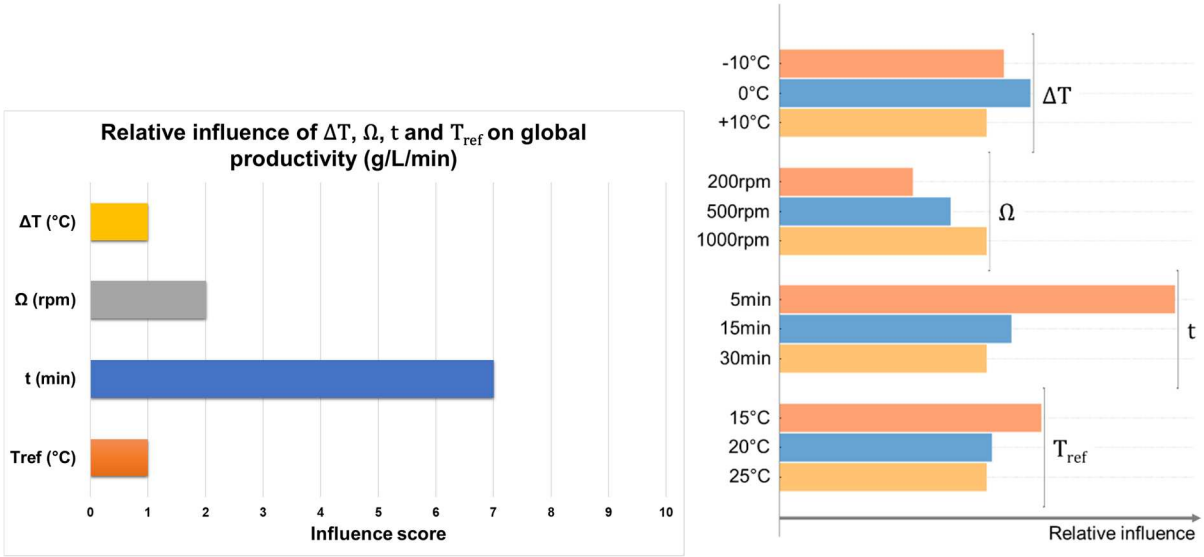

(a) **(b)**

Figure 5: Results from Azurad® for global productivity: (a) Relative influence of the temperature difference ΔT, the rotation speed Ω, the residence time t and the reference temperature T_{ref} on the global productivity. (b) Total effect plot taken from Azurad®; for every factor, the bars give the relative effect of each level to improve global productivity.

The apparent best parameters to improve global productivity are: $\Delta T = 0\,°C$, $\Omega = 1000$ rpm, $t = 5$ min and $T_{ref} = 15\,°C$. It has been performed in repeated experiments 12 R1 and 12 R2, which indeed resulted in excellent global productivities (Table 4).

In batch mode, the global productivity varies from 0.080 g/L/min to 0.242 g/L/min, which means that the continuous mode brings an outstanding increase of at least 16 times. This is far above the examples of transfer from batch mode to continuous mode found in the literature (Kim, 2014; Simon et al., 2019; Lorenz et al., 2020).

4.1.2 Global yield

According to the analysis of the residues, experiment 13 appears to be aberrant in the processing of the global yield results. This complementary experiment can be removed from the experimental matrix, without degrading the quality criteria. The regression model (discarding experiment 13) is very significant with a p-value of 0.2 % and a R^2 of 0.908. The lack of fit is not significant with a p-value of 77.82 %. For global yield, the experimental results and the screening model fit quite well.

As shown in Figure 6a, the two main impacting factors on the global yield are the temperature gradient ΔT and the residence time t. The reference temperature T_{ref} has also some influence. The rotation speed Ω does not seem to have any impact on global yield.

The impact of each factor level on the increase of global yield can be found in Figure 6b. The interpretation should be modulated regarding the influence of each factor discussed before.

When looking at the most impacting factor, residence time, it appears that when it is decreased, the global yield increases. As explained in section 4.1.1, the cooling rate is higher at small residence times, which increases the nucleation rate, but also broaden the PSD.

The second most influential factor is the temperature difference ΔT. The use of the isothermal mode ($\Delta T = 0$ °C) seems to be the best option to improve the global yield. Like for global productivity, nucleation occurs at a higher supersaturation when the temperature gradient is increased (Wu et al., 2017). Moreover, among the two non-isothermal modes, the one with the cold inner cylinder and the hot outer cylinder ($\Delta T = -10$ °C) gives better results. This difference of results according to the non-isothermal mode has already been reported (Wu et al., 2015). It is linked to the driving forces of dissolution and recrystallization exerted respectively in the heating part boundary layer and in the cooling part boundary layer. The temperature regulation of each cylinder may not be equally efficient, which can explain why one non-isothermal mode seems better than the other.

Likewise the global productivity, the decrease of T_{ref} has a positive effect on the global yield.

Apparently, the best level for rotation speed seems to be 500 rpm, but as shown in Figure 6a, this factor has a limited effect on the global yield.

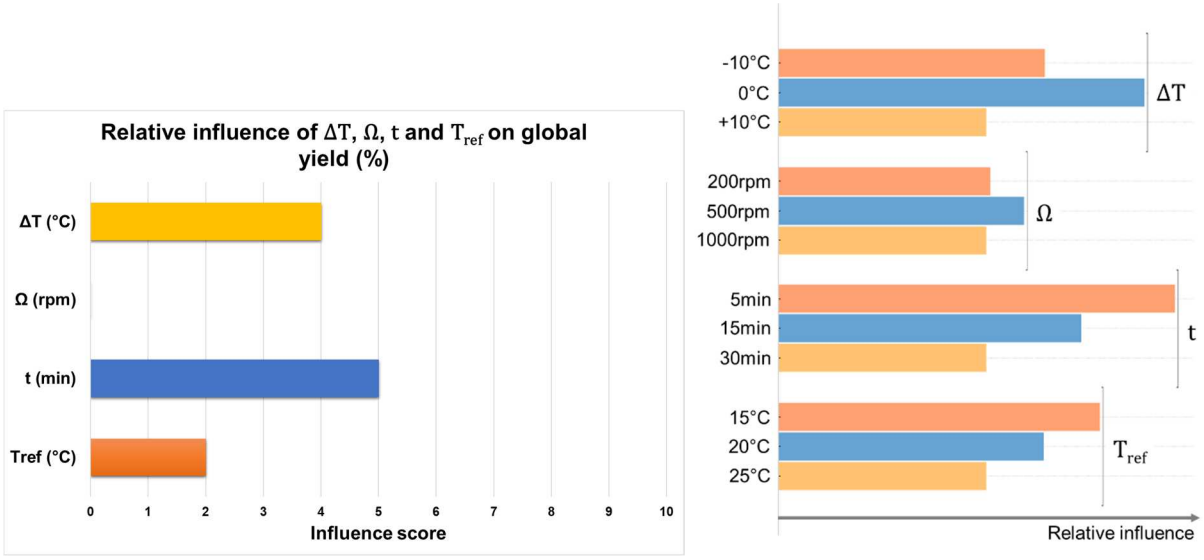

Figure 6: Results from Azurad® for global yield: (a) Relative influence of the temperature difference ΔT, the rotation speed Ω, the residence time t and the reference temperature T_{ref} on the global yield. (b) Total effect plot taken from Azurad®; for every factor, the bars give the relative effect of each level to improve global yield.

The apparent best set of parameters to improve global yield is: $\Delta T = 0$ °C, $t = 5$ min and $T_{ref} = 15$ °C. This set of parameters has been repeated twice: in experiments 12 R1 and 12 R2, which indeed gave excellent global yields (Table 4).

In batch mode, the global yield ranges from 31.4 % to 44.9 %. Even the best results obtained in continuous mode are about 2 times lower. To make sure that the maximum amount of product has been recovered, the mother liquors have been kept at room temperature for 2 days. It did not lead to any precipitation, which means that close to the highest yield was achieved for the starting concentration.

These results are not surprising as it has already been reported that continuous processes trend to give lower yield than batch ones (Zhang et al., 2017; Wood et al., 2019).

However, as the global productivity is very good (see section 4.1.1), an interesting solution could be to implement a recycling system of the mother liquors in a lower domain of temperatures, which has already proven its efficiency regarding yield (Wang et al., 2017; Lorenz et al., 2020; Ma et al., 2020).

4.1.3 Diastereomeric excess

The regression model given by Azurad® is very significant with a p-value near to 0 % and a R^2 of 0.92. The pure error between repeated experiments is very low but the lack of fit is significant, with a p-value of 1.36 %. It means that a small part of variability is not explained by the model. This could be due to interaction effects between parameters.

As shown in Figure 7a, the temperature difference ΔT and the rotation speed Ω are the two most impacting factors on diastereomeric excess. The reference temperature T_{ref} has

also a small influence. Finally, the residence time t has a poor impact on the diastereomeric excess.

The impact of each factor level on the increase of the diastereomeric excess can be found in Figure 7b. The interpretation should be moderated regarding the influence of each factor discussed before.

The most influential parameter is the rotation speed, but its effect seems highly non-linear. This may be explained by potential interactions with other factors. The best rotation speed level to improve the diastereomeric excess is 1000 rpm.

The second most impacting factor is the temperature difference: it clearly appears that the use of CT in non-isothermal mode with the inner cylinder as the cold part and the outer cylinder as the hot one gives the best results of chiral purity. The presence of a temperature gradient was expected to improve chiral purity, as it has already proved its efficiency in deracemization processes (Kim et al., 2017; Schindler, 2020). The reverse non-isothermal mode should be avoided. Such difference between the two non-isothermal modes has already been reported (Wu et al., 2015).

Then, T_{ref} gives a better diastereomeric excess when it decreases, but shows a sort of limit at 20 °C. The same phenomenon is observed for the residence time with 15 min. Again, this behavior may be clarified by studying the interactions between the different factors.

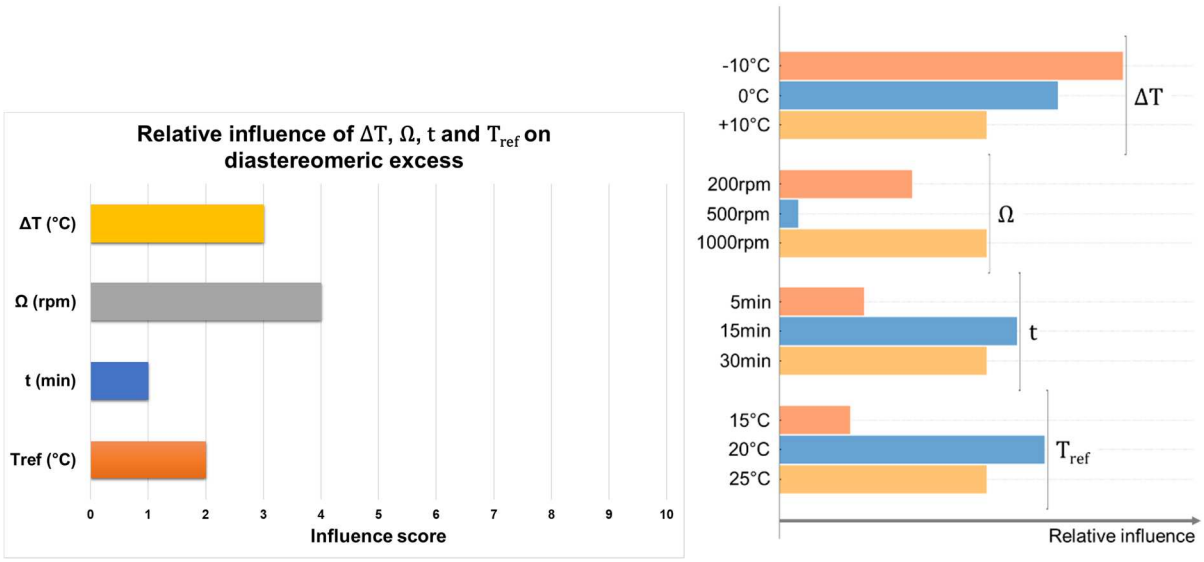

(a) **(b)**

Figure 7: Results from Azurad® for diastereomeric excess: (a) Relative influence of the temperature difference ΔT, the rotation speed Ω, the residence time t and the reference temperature T_{ref} on the diastereomeric excess. (b) Total effect plot taken from Azurad®; for every factor, the bars give the relative effect of each level to improve the diastereomeric excess.

The apparent best parameter set to improve chiral purity is: ΔT = -10 °C, Ω = 1000 rpm, t = 15 min and T_{ref} = 20 °C. Such experiment has not been performed, but the experiments 11

R1 and 11 R2 are quite close ($T_{ref} = 25$ °C) and resulted in the best diastereomeric excess (Table 4).

The chiral purity varies from 0.50 to 0.70 in batch mode, with an average of 0.59. The temperature gradient of the CT crystallizer, combined with its highly efficient mixing, gives better diastereomeric excess in a very repeatable manner (see repeated experiments in Table 4).

It is important to mention that the system Ibu-S-αMBA exhibits a partial solid solution enriched in S-Ibu-S-αMBA (Marc et al., 2021). The limit of miscibility of this solid solution at 20 °C is 13 % of R-Ibu-S-αMBA; therefore, achieving a diastereomeric excess higher than 0.74, in a single operation, may be tricky.

4.1.4 Diastereomeric productivity

According to the analysis of the residues, experiment 13 appears to be aberrant in the processing of the diastereomeric productivity results. This complementary experiment can be removed from the experimental matrix, without degrading the quality criteria. The regression model (discarding experiment 13) is very significant with a p-value of 0.01 % and a R^2 of 0.956. The lack of fit is not significant with a p-value of 30.06 %. For diastereomeric productivity, the experimental results and the screening model fit quite well.

Like the global productivity, the diastereomeric productivity is mainly impacted by the residence time t (Figure 8a). The temperature difference ΔT also has an influence, but it is small. The rotation speed Ω and the reference temperature T_{ref} do not seem to have any impact.

The impact of each factor level on the increase of the diastereomeric productivity can be found in Figure 8b. The interpretation should be modulated regarding the influence of each factor discussed before.

Like for global productivity, the predominance of $t = 5$ min as diastereomeric productivity enhancer seems clear. As explained in section 4.1.1, the cooling rate is higher at small residence times, which increases the nucleation rate. The lower the residence time the higher the diastereomeric productivity.

The second factor with influence is the temperature difference. The use of the isothermal mode ($\Delta T = 0$ °C) seems to be the best option to improve the diastereomeric productivity. Indeed, when the temperature gradient is increased, nucleation occurs at higher supersaturation (Wu et al., 2017), which can affect productivity. Also, among the two non-isothermal modes, the one with the cold inner cylinder ($\Delta T = -10$ °C with the outer hot cylinder) gives better results. This difference of results according to the non-isothermal mode has already been reported (Wu et al., 2015). The influence of ΔT on diastereomeric

productivity is more similar to its impact on global productivity than on diastereomeric excess (see sections 4.1.1 and 4.1.3).

The levels of the factors Ω and T_{ref} are not easy to evaluate, but as explained above, they do not seem to impact the diastereomeric productivity.

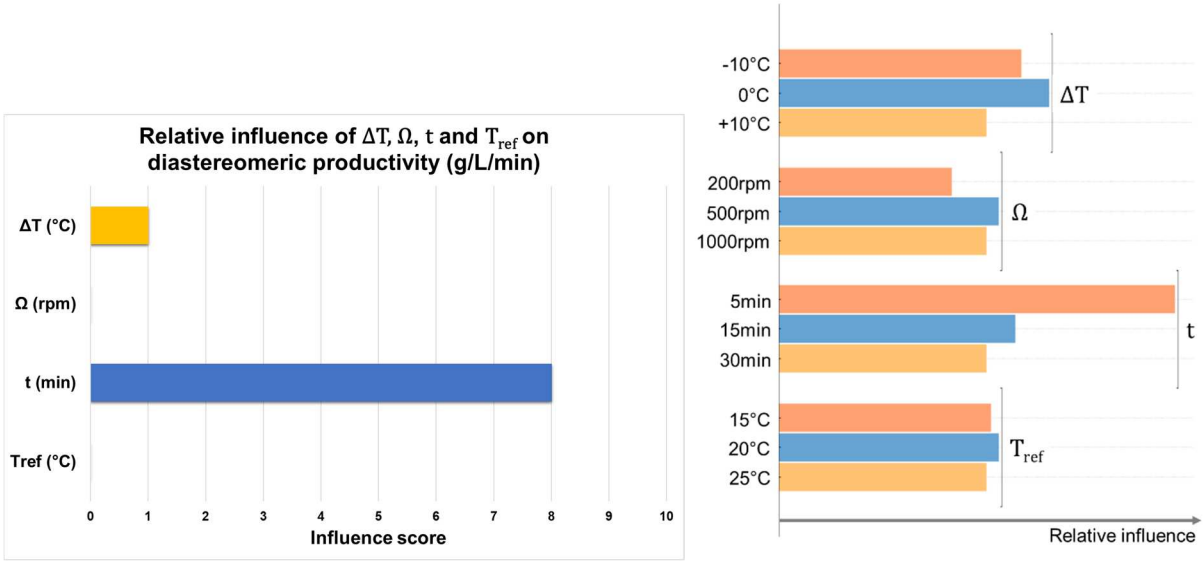

(a) **(b)**

Figure 8: Results from Azurad® for diastereomeric productivity: (a) Relative influence of the temperature difference ΔT, the rotation speed Ω, the residence time t and the reference temperature T_{ref} on the diastereomeric productivity. (b) Total effect plot taken from Azurad®; for every factor, the bars give the relative effect of each level to improve the diastereomeric productivity.

To conclude, the use of $\Delta T = 0\,°C$ and $t = 5\,min$ is the most important to improve diastereomeric productivity. The use of this parameter set in experiments 8, 12 R1 and 12 R2, gave excellent diastereomeric productivities (Table 4). Thus, the influence of ΔT, Ω, t and T_{ref} on diastereomeric productivity is closer to that on global productivity than on diastereomeric excess.

In batch mode, diastereomeric productivity varies from 0.056 g/L/min to 0.121 g/L/min. The use of continuous mode can improve it by, at least, 8 times.

4.1.5 Diastereomeric yield

According to the analysis of the residues, experiments 11R1 and 13 appear to be aberrant in the processing of the diastereomeric productivity results. These complementary experiments can be removed from the experimental matrix, without degrading the quality criteria. The regression model (discarding experiments 11R1 and 13) is significant with a p-value of 0.56 % and a R^2 of 0.905. The lack of fit is not significant with a p-value of 18.71 %. For diastereomeric yield, the experimental results and the screening model fit quite well.

Only two factors seem to have an influence on the diastereomeric yield: the temperature difference ΔT and the residence time t (Figure 9a). The rotation speed Ω and the reference temperature T_{ref} do not seem to have any impact.

The impact of each factor level on the increase of the diastereomeric yield can be found in Figure 9b. The interpretation should be moderated regarding the influence of each factor discussed before.

Regarding the factor ΔT, the use of the isothermal mode (ΔT = 0 °C) seems to be the best option to improve the diastereomeric yield. Like for productivities and global yield, it can be explained because nucleation occurs at a higher supersaturation when the temperature gradient is increased (Wu et al., 2017). Also, among the two non-isothermal modes, the one with the cold inner cylinder (ΔT = -10 °C with the hot outer cylinder) gives better results. Wu et al. (2015) already reported such difference.

Concerning the residence time t, as it decreases, the diastereomeric yield increases. This effect is the same as for productivities and global yield (see sections 4.1.1, 4.1.2 and 4.1.4).

Some trends could be found for Ω and T_{ref}, but their influence on diastereomeric yield is apparently non-existent in the domain explored (Figure 9a).

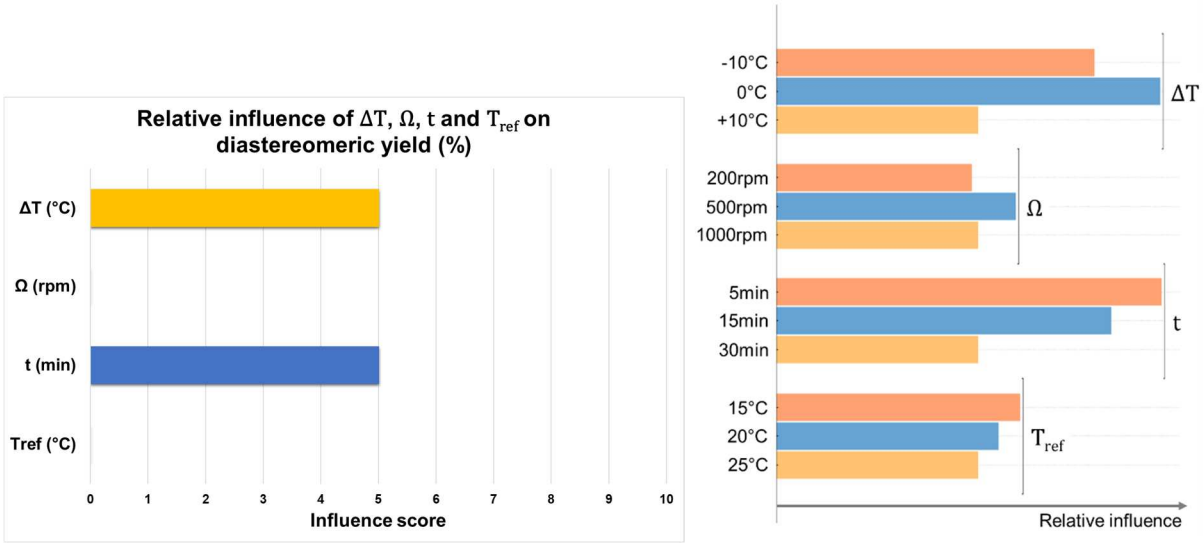

Figure 9: Results from Azurad® for diastereomeric yield: (a) Relative influence of the temperature difference ΔT, the rotation speed Ω, the residence time t and the reference temperature T_{ref} on the diastereomeric yield. (b) Total effect plot taken from Azurad®; for every factor, the bars give the relative effect of each level to improve the diastereomeric yield.

To conclude, the use of ΔT = 0 °C and t = 5 min seems to be the most important to improve diastereomeric yield. This parameter set has been used in experiments 8, 12 R1 and 12 R2, which indeed resulted in good diastereomeric yields (Table 4). In a general way, the influence of ΔT, Ω, t and T_{ref} on diastereomeric yield is closer to that on global yield than on diastereomeric excess.

Batch mode diastereomeric yields range from 22.0 % to 25.7 %. Like for the results of global yield, the best results obtained in continuous mode are about 2 times lower. Again, this outcome is not surprising, and the use of a recycling system of the mother liquors at a lower temperature, could be an efficient solution (see section 4.1.2).

4.2 Conclusions about the studied factors

4.2.1 Temperature difference ΔT

Temperature difference and residence time are the two factors which have an influence on every studied response. The temperature gradient between the two cylinders mainly impacts global yield, global productivity and diastereomeric excess.

The use of CT crystallizer in isothermal mode ($\Delta T = 0$ °C) seems to enhance productivity and yield. It can be explained because the increase of the temperature difference leads to a nucleation occurrence at higher supersaturation (Wu et al., 2017).

However, the non-isothermal mode has a clear influence on diastereomeric excess. Best diastereomeric excess was obtained when the inner cylinder was the cold part, ($\Delta T = -10$ °C with the outer hot cylinder). This non-isothermal mode also gives good results in terms of productivity and yield. The reverse mode (hot inner cylinder and cold outer cylinder) did not lead to any response improvement. The difference of results according to the non-isothermal mode has been reported by Wu et al. (2015). It is linked to the driving forces of dissolution and recrystallization exerted respectively in the heating part boundary layer and in the cooling part boundary layer. The temperature regulation of each cylinder may not be equally efficient, which can explain why one non-isothermal mode appears to be better than the other.

For further studies, the non-isothermal mode implying the inner cylinder as the cold part and the outer as the hot part will be preferred, regarding its positive impact on diastereomeric excess, productivity, and yield. Also, the range of studied ΔT should be extended.

4.2.2 Rotation speed Ω

The rotation speed seems to have an impact on global productivity and diastereomeric excess. In both cases, the level 1000 rpm increased the response. The positive effect of the rotation speed increase can be explained by an enhancement of heat and mass transfer rates. The enhanced mass transfer leads to productivity improvement. Diastereomeric excess is strongly impacted by the presence of a temperature gradient; because of the increased heat transfer, the efficiency of the temperature difference is also improved (Wu et al., 2015), leading to a higher chiral purity.

Rotation speed did not appear to have a real influence on the other responses.

In the further work, it will be fixed at 1000 rpm.

4.2.3 Residence time t

The residence time has an influence on every response. Its impact is strong on productivity and yield. The best results were obtained at t = 5 min. More generally, when the residence time decreases, the productivity and the yield increase. At small residence times, the cooling is faster, which increases the nucleation rate, thus the yield and the productivity. However, the side effect is a broader PSD, i.e., a less homogeneous powder.

Nevertheless, this factor should be carefully handled regarding chiral purity. Indeed, 5 min of residence time resulted in low diastereomeric excesses. A compromise can be found by using 10 min for example. Anyway, the value 30 min will be eliminated in the future work.

4.2.4 Reference temperature T_{ref} (target temperature within the CT crystallizer)

The reference temperature has an impact on global productivity, global yield and diastereomeric excess. Regarding global productivity and global yield, the decrease of T_{ref} leads to an increase of both responses. This trend was expected, as the decrease of temperature leads to an increase in supersaturation.

For the diastereomeric excess, the effect is less intuitive. Up to 20 °C, the diminution of T_{ref} improves the chiral purity, but the lowest level 15 °C resulted in poor diastereomeric excesses.

No levels can reasonably be eliminated at this stage. The study of this factor through a surface response design should be more conclusive.

4.3 Unusual yield behavior

Previous results in pure ethanol predicted a fast reach of the steady state functioning in the CT crystallizer (Figure 4, section 3.3). However, in the present work, during the execution of the DoE experiments, some unexpected yield behavior has been encountered.

As shown in Figure 10, from fraction 1 F1 to fraction 10 F10, this strange yield pattern is repeatable from one experiment to another, in the same process conditions. Regarding that, three experiments have been performed during 20 residence times instead of 10, to see if this peculiarity was due to fouling or if it was a matter of steady state. Those are experiments 11 R2, 12 R2 and 14 (Table 3).

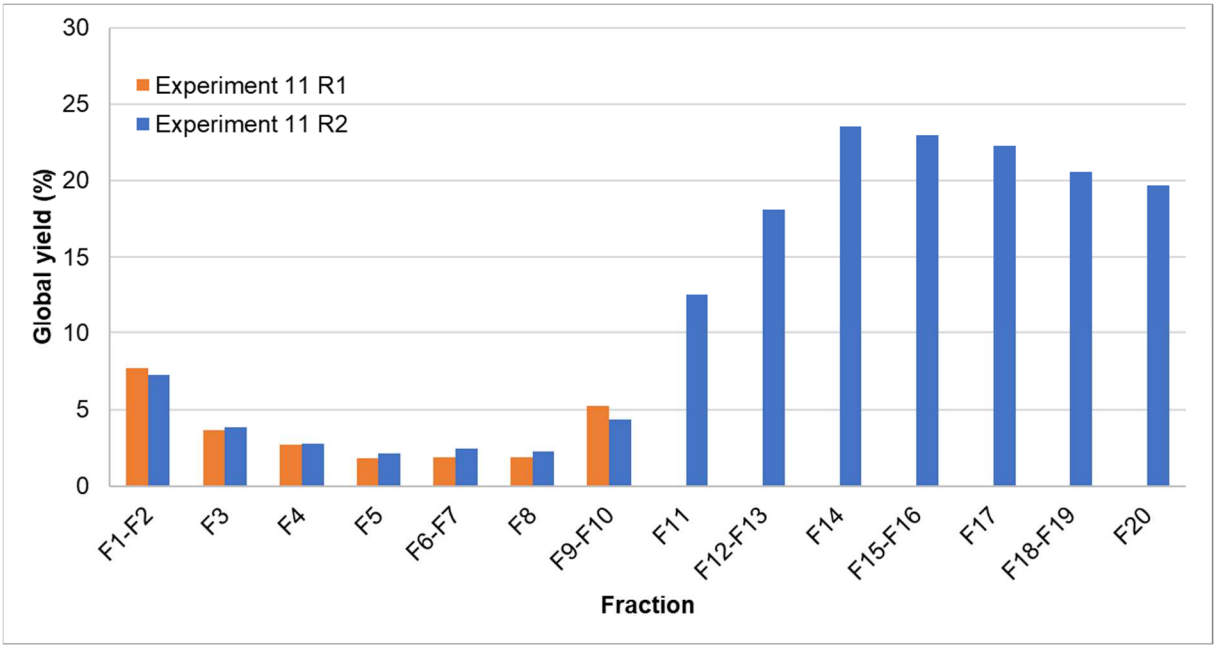

Figure 10: Global yield histogram for experiments 11 R1 (orange) and 11 R2 (blue). Experiment 11 R1 lasted 10 residence times and experiment 11 R2 lasted 20 residence times.

From these experiments, the hypothesis is that in the used process conditions, steady state is not reached as soon as in the previous work in pure ethanol. It seems to be achieved after 14-15 residence times.

Also, it seems that yield and productivity are strongly enhanced when the steady state is reached. Chiral purity remains stable from 1 to 20 residence times.

Regarding that, the interpretation of the DoE has been checked. It appeared that the trends identified for every studied factor remain identical.

Further experiments should be set up for at least 20 residence times to ensure the attainment of the steady state.

5 Conclusions

In the presented work, continuous chiral resolution of rac-Ibu by diastereomeric salt formation has been successfully implemented in a CT crystallizer. To determine the best process conditions, seven parameters were identified as interesting to study:

- (1) Absolute temperature difference between the two cylinders $|\Delta T|$,
- (2) Sign of ΔT, i.e., which cylinder is the cold part when the other is the hot one,
- (3) Rotation speed Ω,
- (4) Residence time t, i.e., flowrate,
- (5) Reference temperature T_{ref}, i.e., target temperature within the CT crystallizer,
- (6) Medium concentration,
- (7) Solvent mass ratio EtOH/H_2O.

In a first place, to make a primary outline of the influence of the different parameters, a screening has been set up with four factors, expected to be the most impacting ones for a constant feed concentration:

- (1)(2) Temperature difference ΔT
- (3) Rotation speed Ω,
- (4) Residence time t, i.e., flowrate,
- (5) Reference temperature T_{ref}, i.e., target temperature within the CT crystallizer.

Thanks to the rationalization of the study through a DoE, 14 distinct experiments were performed out of 81 possible experiments, to identify the influence of the four main factors on global and diastereomeric productivities and yields, and on diastereomeric excess.

The temperature difference between the two cylinders has an impact on every studied response. The use of the CT crystallizer in isothermal mode ($\Delta T = 0$ °C) seems to enhance productivity and yield compared to the use in non-isothermal mode. However, the non-isothermal mode with the inner cylinder as the cold part and the outer cylinder as the hot one, has a clear positive influence on diastereomeric excess.

Rotation speed has an impact on global productivity and diastereomeric excess, with an optimized level of 1000 rpm, to ensure improved heat and mass transfer rates.

Residence time has a strong influence on productivity and yield: when the residence time decreases, the productivity and the yield increase. However, a too short residence time disadvantages the diastereomeric excess. A compromise should be found in further studies to guarantee good chiral purity, productivity and yield at the same time.

Regarding the reference temperature T_{ref}, when it decreases, global productivity and global yield increases. This is due to the increase of supersaturation when the temperature decreases. For the diastereomeric excess, the effect of T_{ref} is less evident.

With the good parameter set, global productivity and diastereomeric productivity were increased by 16 and 8 times respectively, in comparison with batch mode. Also, continuous mode gives an easy access to a higher diastereomeric excess, in a very repeatable manner. Concerning the global yield and diastereomeric yield, the obtained results are lower than in batch mode. However, as the productivity is very good, an interesting solution could be the implementation of a recycling system of the mother liquors. Moreover, the latest experiments, performed on longer operating time, show that the evaluated yield may be underestimated, especially in case of favorable conditions for diastereomeric excess.

Indeed, an unusual behavior was encountered regarding the yield during the experiments. The hypothesis is that steady state was not reached as soon as in previous work in pure ethanol. When it is achieved, after 14 to 15 residence times, it seems that yield

and productivity are strongly enhanced. Diastereomeric excess remains stable from the beginning to the end of the experiments.
Further experiments should be set up for at least 20 residence times.

After this first screening, the factors and their range of settings will be readjusted. The rotation speed can be fixed as well as the non-isothermal mode for ΔT. Further work should go through a new design of experiments, integrating the parameters not yet studied (medium concentration and solvent composition) as well as factor effect interaction. While the work with the DoE is progressing, the influence of the seven identified parameters will be mapped. A response surface should be drawn with the few most critical parameters to identify a robust operating point.
In the end, thanks to this rationalized study, it will be possible to understand the levers of this crystallization system, and potentially answer any request regarding: global productivity, diastereomeric productivity, yield and diastereomeric excess. Depending on to the need, the model established with the DoE will determine the ideal set of parameters to meet it (in the studied range).

Acknowledgements

Prof. Woo-Sik Kim (Kyung Hee University, South-Korea) is thanked for his help in the critical Taylor number calculation. Jean-Yves Lenoir and Edouard Rebmann (Seqens, France) are thanked for their help in the design of the mixing chamber of the continuous set-up. Charles Lanel (University of Rouen Normandie, France) is thanked for his time and his help to design and manufacture the mixing chamber. Finally, Chrystal Lopes (Master trainee) is thanked for her contribution to the experimental work.

Pharmadev (Geneva CH) is thanks for the free supply of rac-Ibu. SEQENS is thanked for PhD support of L.M.

Abbreviations

API: Active Pharmaceutical Ingredient
CT: Couette-Taylor
de: diastereomeric excess
DoE: Design of Experiments
F: Fraction
GRAS: Generally Regarded As Safe
HPLC: High Performance Liquid Chromatography
MSMPR: Mixed-Suspension, Mixed-Product Removal
PC: Preferential Crystallization

PFC: Plug Flow Crystallizer

PSD: Particle Size Distribution

R: Repetition

R-Ibu: R-(-)-Ibuprofen

R-Ibu-S-αMBA: R-(-)-Ibuprofen-S-(-)-α-Methylbenzylamine

RA: Resolving Agent

rac-Ibu: Racemic Ibuprofen

rpm: rotation per minute

S-αMBA: S-(-)-α-Methylbenzylamine

S-Ibu: S-(+)-Ibuprofen

S-Ibu-S-αMBA: S-(+)-Ibuprofen-S-(-)-α-Methylbenzylamine

XRPD: X-Ray Powder Diffraction

Nomenclature

Symbol	Name (Unit)
d	Gap between the two cylinders (m)
$m_{collected}$	Mass of solid recovered from V during $t_{collection}$ (g)
$m_{expected}$	Maximum mass of solid that can be recovered from V during $t_{collection}$ (g)
p	Variance (%)
R^2	Correlation coefficient (-)
Re_z	Longitudinal Reynolds number (flow) (-)
r_i	Inner cylinder radius (m)
r_o	Outer cylinder radius (m)
t	Residence time (min)
$T1$	Set temperature of the thermostat of the inner cylinder (°C)
$T2$	Set temperature of the thermostat of the outer cylinder (°C)
Ta	Taylor number (-)
Ta^*_c	Critical Taylor number with an axial flow (-)
$Ta^*_c\ (Re_z=0)$	Critical Taylor number without axial flow (-)
$t_{collection}$	Duration of the fraction collection (min)
T_j	Set temperature of the jacket (°C)
T_{ref}	Reference temperature T_{ref}, i.e., target temperature within the CT crystallizer (°C)
V	Volume of suspension collected during $t_{collection}$ (L)
V_m	Mean axial linear velocity (m/s)
ΔT	Temperature difference (°C)

η Radius ratio (-)

ν Kinematic viscosity (m^2/s)

Ω Rotation speed (rpm)

Ω_i Rotation speed of the inner cylinder (rad/s)

References

Badman, C., Cooney, C.L., Florence, A., Konstantinov, K., Krumme, M., Mascia, S., Nasr, M., Trout, B.L., 2019. Why We Need Continuous Pharmaceutical Manufacturing and How to Make It Happen. J. Pharm. Sci. 108, 3521–3523. https://doi.org/10.1016/j.xphs.2019.07.016

Baumann, M., Moody, T.S., Smyth, M., Wharry, S., 2020. A Perspective on Continuous Flow Chemistry in the Pharmaceutical Industry. Org. Process Res. Dev. 24, 1802–1810. https://doi.org/10.1021/acs.oprd.9b00524

Bhattacharya, A., Murphy, D., 2003. Temperature Selective Diastereo-Recognition (TSD): Enantiomeric Ibuprofen via Environmentally Benign Selective Crystallization. Org. Process Res. Dev. 7, 717–722. https://doi.org/10.1021/op030203i

Carvalho, P.O., Cass, Q.B., Calafatti, S.A., Contesini, F.J., Bizaco, R., 2006. Review-Alternatives for the separation of drug enantiomers: ibuprofen as a model compound. Braz. J. Chem. Eng. 23, 291–300. https://doi.org/10.1590/S0104-66322006000300003

Chandrasekhar, S., 1961. Chapter VII The stability of Couette Flow, in: Chandrasekhar, S. (Ed.), Hydrodynamic and Hydromagnetic Stability. Clarendon Press: Oxford University Press, Oxford, pp. 272–342.

Cole, K.P., Johnson, M.D., 2018. Continuous flow technology vs. the batch-by-batch approach to produce pharmaceutical compounds. Expert Rev. Clin. Pharmacol. 11, 5–13. https://doi.org/10.1080/17512433.2018.1413936

Coquerel, G., 2015. Chiral Discrimination in the Solid State: Applications to Resolution and Deracemization, in: Tamura, R., Miyata, M. (Eds.), Advances in Organic Crystal Chemistry: Comprehensive Reviews 2015. Springer Japan, Tokyo, pp. 393–420. https://doi.org/10.1007/978-4-431-55555-1_20

Couette, M., 1890. Distinction de deux régimes dans le mouvement des fluides. J. Phys. Theor. Appl. 9, 414–424. https://doi.org/10.1051/jphystap:018900090041401

Donnelly, R.J., Schwarz, K.W., 1965. Experiments on the stability of viscous flow between rotating cylinders - VI. Finite-amplitude experiments. Proc. R. Soc. Lond. A 283, 531–556. https://doi.org/10.1098/rspa.1965.0044

Evans, A.M., 2001. Comparative Pharmacology of S(+)-Ibuprofen and (RS)-Ibuprofen. Clin. Rheumatol. 20, 9–14. https://doi.org/10.1007/BF03342662

Faigl, F., Fogassy, E., Nógrádi, M., Pálovics, E., Schindler, J., 2008. Strategies in optical resolution: a practical guide. Tetrahedron: Asymmetry 19, 519–536. https://doi.org/10.1016/j.tetasy.2008.02.004

Fogassy, E., Nógrádi, M., Kozma, D., Egri, G., Pálovics, E., Kiss, V., 2006. Optical resolution methods. Org. Biomol. Chem. 4, 3011–3030. https://doi.org/10.1039/b603058k

Hermans, T.M., Sato, A., Marichez, V., 2017. Method for chiral resolution and device therefor.

Hughes, D.L., 2020. Applications of Flow Chemistry in the Pharmaceutical Industry—Highlights of the Recent Patent Literature. Org. Process Res. Dev. 24, 1850–1860. https://doi.org/10.1021/acs.oprd.0c00156

Hughes, D.L., 2018. Applications of Flow Chemistry in Drug Development: Highlights of Recent Patent Literature. Org. Process Res. Dev. 22, 13–20. https://doi.org/10.1021/acs.oprd.7b00363

Kang, S.H., Lee, S.G., Jung, W.M., Kim, M.C., Kim, W.-S., Choi, C.K., Feigelson, R.S., 2003. Effect of Taylor vortices on calcium carbonate crystallization by gas–liquid reaction. J. Cryst. Growth 254, 196–205. https://doi.org/10.1016/S0022-0248(03)01152-7

Kataoka, K., 1986. CHAPTER 9. TAYLOR VORTICES AND INSTABILITIES IN CIRCULAR COUETTE FLOWS, in: Cheremisinoff, N.P. (Ed.), Encyclopedia Of Fluid Mechanics Vol-1. Houston, pp. 237–274.

Kim, W.-S., 2014. Application of Taylor Vortex to Crystallization. J. Chem. Eng. Japan 47, 115–123. https://doi.org/10.1252/jcej.13we143

Kim, W.-S., Yu, T., Whu, Z., 2017. Method for conductiong deracemization using Taylor flow and a device therefor. 10,106,408.

Lemmerer, A., Bourne, S.A., Caira, M.R., Cotton, J., Hendricks, U., Peinke, L.C., Trollope, L., 2010. Incorporating active pharmaceutical ingredients into a molecular salt using a chiral counterion. CrystEngComm 12, 3634. https://doi.org/10.1039/c0ce00043d

Liu, Y.C., Domokos, A., Coleman, S., Firth, P., Nagy, Z.K., 2019. Development of continuous filtration in a novel continuous filtration carousel integrated with continuous crystallization. Org. Process Res. Dev. 23, 2655–2665. https://doi.org/10.1021/acs.oprd.9b00342

Long, W.S., Kamaruddin, A., Bhatia, S., 2005. Chiral resolution of racemic ibuprofen ester in an enzymatic membrane reactor. J. Membr. Sci. 247, 185–200. https://doi.org/10.1016/j.memsci.2004.09.019

Lorenz, H., Temmel, E., Seidel-Morgenstern, A., 2020. The Handbook of Continuous Crystallization CHAPTER 12 Continuous Enantioselective Crystallization of Chiral Compounds, in: Yazdanpanah, N., Nagy, Z.K. (Eds.), The Handbook of Continuous Crystallization. The Royal Society of Chemistry, pp. 422–468. https://doi.org/10.1039/9781788013581-00422

Ma, Y., Wu, S., Macaringue, E.G.J., Zhang, T., Gong, J., Wang, J., 2020. Recent Progress in Continuous Crystallization of Pharmaceutical Products: Precise Preparation and Control. Org. Process Res. Dev. 24, 1785–1801. https://doi.org/10.1021/acs.oprd.9b00362

Marc, L., Lopes, C., Schneider, J.-M., Sanselme, M., Coquerel, G., 2021. Impact of a Partial Solid Solution and Water Molecules on the Formation of Fibrous Crystals and Fluid Inclusions. Crystals 11, 1188. https://doi.org/10.3390/cryst11101188

Marichez, V., Tassoni, A., Cameron, R.P., Barnett, S.M., Eichhorn, R., Genet, C., Hermans, T.M., 2019. Mechanical chiral resolution. Soft Matter 15, 4593–4608. https://doi.org/10.1039/C9SM00778D

Maron, D.M., Cohen, S., 1991. Hydrodynamics and Heat/Mass Transfer near Rotating Surfaces, in: Hartnett, J.P., Irvine, T.F., Cho, Y.I. (Eds.), Advances in Heat Transfer. Elsevier, pp. 141–183. https://doi.org/10.1016/S0065-2717(08)70335-6

Nguyen, A.-T., Joo, Y.L., Kim, W.-S., 2012. Multiple Feeding Strategy for Phase Transformation of GMP in Continuous Couette–Taylor Crystallizer. Cryst. Growth Des. 12, 2780–2788. https://doi.org/10.1021/cg201361e

Nguyen, A.-T., Kim, J.-M., Chang, S.-M., Kim, W.-S., 2010. Taylor Vortex Effect on Phase Transformation of Guanosine 5-Monophosphate in Drowning-Out Crystallization. Ind. Eng. Chem. Res. 49, 4865–4872. https://doi.org/10.1021/ie901932t

Nguyen, A.-T., Yu, T., Kim, W.-S., 2017. Couette-Taylor crystallizer: Effective control of crystal size distribution and recovery of l-lysine in cooling crystallization. J. Cryst. Growth 469, 65–77. https://doi.org/10.1016/j.jcrysgro.2016.10.020

Park, S.-A., Lee, S., Kim, W.-S., 2015. Polymorphic Crystallization of Sulfamerazine in Taylor Vortex Flow: Polymorphic Nucleation and Phase Transformation. Cryst. Growth Des. 15, 3617–3627. https://doi.org/10.1021/acs.cgd.5b00002

Rivera, N.R., Kassim, B., Grigorov, P., Wang, H., Armenante, M., Bu, X., Lekhal, A., Variankaval, N., 2019. Investigation of a Flow Step Clogging Incident: A Precautionary Note on the Use of THF in Commercial-Scale Continuous Process. Org. Process Res. Dev. 23, 2556–2561. https://doi.org/10.1021/acs.oprd.9b00366

Rogers, L., Jensen, K.F., 2019. Continuous manufacturing – the Green Chemistry promise? Green Chem. 21, 3481–3498. https://doi.org/10.1039/C9GC00773C

Sánchez, A., Valero, F., Lafuente, J., Solà, C., 2000. Highly enantioselective esterification of racemic ibuprofen in a packed bed reactor using immobilised Rhizomucor miehei lipase. Enzyme Microb. Technol. 27, 157–166. https://doi.org/10.1016/S0141-0229(00)00207-6

Schindler, M., 2020. Deracémisation du chlorate de sodium avec et sans l'influence du dithionate de sodium (thesis). http://www.theses.fr. Normandie.

Siedlecka, R., 2013. Recent developments in optical resolution. Tetrahedron 69, 6331–6363. https://doi.org/10.1016/j.tet.2013.05.035

Simon, M., Wood, B., Ferguson, S., Glennon, B., Jones, R.C., 2019. Diastereomeric salt crystallization of chiral molecules via sequential coupled-Batch operation. AIChE J 65, 604–616. https://doi.org/10.1002/aic.16466

Sparrow, E.M., Munro, W.D., Jonsson, V.K., 1964. Instability of the flow between rotating cylinders: the wide-gap problem. J. Fluid Mech. 20, 35–46. https://doi.org/10.1017/S0022112064001008

Taylor, G.I., 1923. Stability of a Viscous Liquid Contained between Two Rotating Cylinders. Phil. Trans. R. Soc. A Philos. Trans. R. Soc. A-Math. Phys. Eng. Sci. 223, 289–343. https://doi.org/10.1098/rsta.1923.0008

Thai, D.K., Mayra, Q.-P., Kim, W.-S., 2015. Agglomeration of Ni-rich hydroxide crystals in Taylor vortex flow. Powder Technol. 274, 5–13. https://doi.org/10.1016/j.powtec.2015.01.008

Viedma, C., Coquerel, G., Cintas, P., 2015. 22 - Crystallization of Chiral Molecules, in: Nishinaga, T. (Ed.), Handbook of Crystal Growth (Second Edition). Elsevier, Boston, pp. 951–1002. https://doi.org/10.1016/B978-0-444-56369-9.00022-8

Wang, T., Lu, H., Wang, J., Xiao, Y., Zhou, Y., Bao, Y., Hao, H., 2017. Recent progress of continuous crystallization. J. Ind. Eng. Chem. 54, 14–29. https://doi.org/10.1016/j.jiec.2017.06.009

Wang, Y., Chen, A., 2013. Crystallization-Based Separation of Enantiomers, in: Andrushko, V., Andrushko, N. (Eds.), Stereoselective Synthesis of Drugs and Natural Products. John Wiley & Sons, Inc., Hoboken, NJ, USA, pp. 1663–1682. https://doi.org/10.1002/9781118596784.ssd056

Wood, B., Girard, K.P., Polster, C.S., Croker, D.M., 2019. Progress to Date in the Design and Operation of Continuous Crystallization Processes for Pharmaceutical Applications. Org. Process Res. Dev. 23, 122–144. https://doi.org/10.1021/acs.oprd.8b00319

Wu, Z., Kim, D.H., Kim, W.-S., 2017. Batch Cooling Crystallization in Non-Isothermal Taylor Vortex Flow: Effective Method for Controlling Crystal Size Distribution. Cryst. Growth Des. 17, 28–36. https://doi.org/10.1021/acs.cgd.6b00821

Wu, Z., Seok, S., Kim, D.H., Kim, W.-S., 2015. Control of Crystal Size Distribution using Non-Isothermal Taylor Vortex Flow. Cryst. Growth Des. 15, 5675–5684. https://doi.org/10.1021/acs.cgd.5b00431

Zhang, D., Xu, S., Du, S., Wang, J., Gong, J., 2017. Progress of Pharmaceutical Continuous Crystallization. Engineering 3, 354–364. https://doi.org/10.1016/J.ENG.2017.03.023